Table 3 Effect of particle size on the ID of amines

Particle size, μ	Average ID, msec: Benzidine, 350 mg; RFNA, 0.5 ml (21.6% NO_2)	Average ID, msec: *p*-phenylenediamine, 300 mg; RFNA, 1 ml (8% NO_2)
453-377	767	205
377-226	580	165
226-180	490	97
180-120	477	...
120-85	640,3227[a]	219, 531[a]

[a] Value corresponding to second flame.

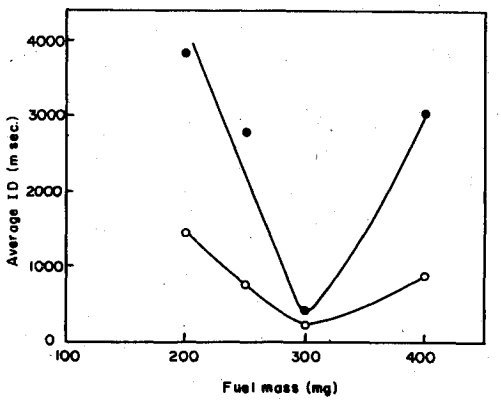

Fig. 2 Effect of relative amounts of fuel and oxidizer on the ignition delays of *p*-phenylenediamine [particle size, 120-80 μ; RFNA, 1 ml (8% NO_2); ○, first flame; ●, second flame].

The variation in ignition delays with the concentration of NO_2 in nitric acid is plotted in Fig. 1. It is seen that FPH and DBPH both give least ignition delays with the pure anhydrous acid, rather than RFNA. The ignition delays are maximum around 12-16% NO_2 concentration in the acid. Figure 1 also shows that the oxidizer/fuel ratio for minimum ignition delays does not change significantly with the NO_2 concentration. The effect of particle size of the fuel on the ID of FPH and DBPH is presented in Table 2. It appears that the ignition delays decrease only marginally up to a certain particle size when one goes from coarse to fine particles. The fuel burns readily in this region, giving highly reproducible ignition delays. The minimum delays are observed at particle sizes of 252-212 and 125-105 μ in the cases of FPH and DBPH, respectively. Below these particle sizes again, longer ignition delays are observed, and the ignition of the fuel becomes erratic. The ID values observed in this fine-particle-size region may be divided into two distinct sets, probably corresponding to two flames. The first flame appears but is not permanent and extinguishes soon. The second flame, which appears later, is steady and lasts until the fuel and/or oxidizer is consumed. The phototransister circuit senses sometimes the first flame and sometimes the second, and therefore two sets of values of the ignition delays are obtained.

A similar effect was observed in the case of amine fuels, benzidine, and *p*-phenylenediamine. As shown in Table 3, the ignition delays of these systems decrease up to a certain particle size, v.z. 150 μ, below which the ignition becomes erratic, resulting in two flames. In the case of benzidine, because of considerable time lag, the two flames could be distinguished visibly by the naked eye and could be photographed using a storage oscilloscope. In order to observe this phenomenon more carefully, we studied the ignition behavior of finely powdered (particle size, 120-85 μ) *p*-phenylenediamine/RFNA system as a function of oxidizer-to-fuel ratio. As expected, two ID values corresponding to two flames are obtained at each oxidizer-to-fuel ratio, as shown in Fig. 2. It therefore appears to be a general phenomenon for fine powders.

References

[1] Jain, S.R., "Ignition and Thermal Behavior of Solid Hydrazones," *Combustion and Flame,* Vol. 28, Feb. 1977, p. 101.

[2] Bernard, M.L., Cointot, A., Auzanneau, M., and Sztal, B., "The Role of Surface Reactions in Hypergolic Ignition of Liquid Solid Systems," *Combustion and Flame,* Vol. 22, Feb. 1974, pp. 1-7.

[3] Rastogi, R.P. and Bisht, M.M.S., "Combustion Processes Occurring between solid fuels and Liquid Oxidizers," *Indian Journal of Chemistry,* Vol. 9, April 1971, pp. 333-338.

[4] Munzal, N.L. and Parvatiyar, M.G., "Ignition of Hybrid Rocket Fuels with Fuming Nitric Acid as Oxidant," *Journal of Spacecraft and Rockets,* Vol. 11, June 1974, pp. 428-430.

Estimate of Pressure Distribution on Launch Vehicles at Small Angles of Attack

M.S. Sastry*
Space Science and Technology Centre, Trivandrum, India

Nomenclature

C_p = coefficient of pressure
C_{p0} = leeward side coefficient of pressure
$C_{p\pi}$ = windward side coefficient of pressure
M = Mach number
X/L = nondimensional axial coordinate
α = angle of attack
γ = specific heat ratio
θ_b = body parameter
θ_v = turning angle
ϕ = circumferential angle

Subscripts

A = location on the body (or afterbody) after acceleration (or expansion) starting point
F = location on the body (or afterbody) before acceleration (or expansion) starting point
∞ = freestream

FRIBERG and Walchner[1] predicted the hypersonic pressure distribution on axisymmetric blunt slender cones for any circumferential angle, using the formula

$$C_p(\phi) = \tfrac{1}{2}\left[(C_{p0}/2)^{1/2}(1+\cos\phi) + (C_{p\pi}/2)^{1/2}(1-\cos\phi)\right]^2 \quad (1)$$

where, for small values of $(\theta_b \pm \alpha)$,

$$C_{p0,\pi} = 2(\theta_b \pm \alpha)^2 \quad (2)$$

The Newtonian impact values of Eq. (2) for the leeward and windward sides were replaced by measured values in their analysis. McBrayer[2] utilized empirical correlation plots and improved the accuracy of the tangent cone method.

In applying these formulas to the blunt nose cose and flare of a launch vehicle, it is assumed that C_p at zero angle of

Received Feb. 22, 1977; revision received April 18, 1977.
Index category: LV/M Aerodynamics.
*Scientist, Aerodynamics Division.

attack is known, so that θ_b as a function of X/L can be obtained from Eq. (2) for a given Mach number and location by setting $\alpha = 0°$. Again reusing Eq. (2) with the desired values of α and the previously determined values of θ_b, the leeward and windward values $C_{p0,\pi}$ can be determined and substituted in Eq. (1) to obtain the entire pressure distribution. The curvature correction suggested by McBrayer[2] has not been used here. This procedure was applied to all Mach number ranges, with satisfactory results.

For the cone-cylinder junction, the Prandtl-Meyer formula for expanding flow is used:

$$C_{pA} = (C_{pF} + 2/\gamma M_\infty^2) X - 2/\gamma M_\infty^2 \tag{3}$$

where usually

$$X = [1 - (\gamma - 1)/2M_F\theta_\nu]^{2\gamma/(\gamma-1)} \tag{4}$$

For purposes of this paper,

$$X = (C_{pA} + 2/\gamma M_\infty^2)/(C_{pF} + 2/\gamma M_\infty^2) \tag{5}$$

for $\alpha = 0°$.

Since M_F and θ_ν are not known for flow with incidence, it is assumed that X does not change significantly with incidence. Thus X can be evaluated with the values of C_{pA} and C_{pF} at $\alpha = 0°$. Now, since C_{pF} for flow with incidence is known, C_{pA} can be evaluated with Eq. (3).

On the cylindrical portion where the flow ceases to expand, the pressure relaxes to the freestream value. Here, an empirical formula is used:

$$\left(\frac{C_{p\text{ previous location}}}{C_{p\text{ present location}}}\right)_{\alpha \neq 0°} = \left(\frac{C_{p\text{ previous location}}}{C_{p\text{ present location}}}\right)_{\alpha = 0°} \tag{6}$$

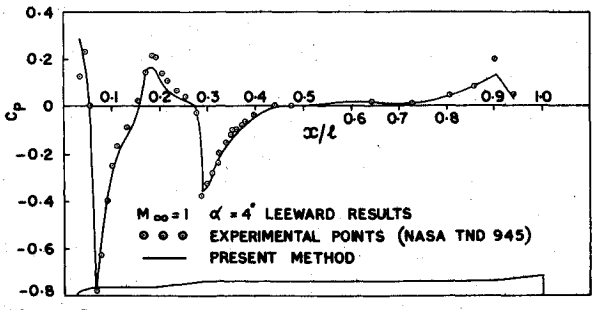

Fig. 1 Pressure distribution for body alone for Mach number 1.

Now Eqs. (1, 3 and 6) can be used to determine the complete pressure distribution on the surface of an axisymmetric blunt cone-cylinder-flare combination at small angles of incidence provided that the distribution for zero incidence is known. Equation (3), which accounts for the flow expansion over the cone-cylinder junction, is applied over values of X/L corresponding to the expansion for zero incidence.

This procedure was applied to the Scout vehicle, and the results are compared with experimental data.[3-5] in Table 1 for the upper cone-cylinder-flare portion of the vehicle for Mach number 2.96. The graphs in Figs. 1 and 2 show comparisons

Table 1 C_p at Mach number 2.96 (Ref. 4 for experimental)

X/L	$C_{p_{\alpha=0°}}$	Method	$\phi=0°$ $\alpha=4°$	$\phi=30°$ $\alpha=4°$	$\phi=60°$ $\alpha=4°$	$\phi=120°$ $\alpha=4°$	$\phi=150°$ $\alpha=4°$	$\phi=180°$ $\alpha=4°$
0.024	1.7259	Exptl.	1.7209	1.6831	1.7047	1.7148	1.7149	1.6724
		Present	1.4762	1.5085	1.5986	1.8580	1.9579	1.9951
0.035	0.2276	Exptl.	0.1547	0.1614	0.1873	0.2668	0.2996	0.3107
		Present	0.1431	0.1533	0.1829	0.2771	0.3165	0.3316
0.045	0.2352	Exptl.	0.1623	0.1728	0.1967	0.2782	0.3090	0.3182
		Present	0.1492	0.1596	0.1898	0.2855	0.3254	0.3407
0.055	0.2164	Exptl.	0.1433	0.1538	0.1836	0.2592	0.2977	0.3145
		Present	0.1344	0.1443	0.1728	0.2641	0.3023	0.3169
0.065	−0.0253	Exptl.	−0.0571	−0.0537	−0.0406	−0.0122	0.0082	0.0088
		Present	−0.0551	−0.0449	−0.0224	0.0004	0.0069	0.0112
0.076	−0.0290	Exptl.	−0.0571	−0.0537	−0.0444	−0.0159	0.0006	0.0031
		Present	−0.0580	−0.0480	−0.0257	0.0000	0.0035	0.0065
0.091	−0.0290	Exptl.	−0.0534	−0.0498	−0.0424	−0.0198	−0.0032	−0.0045
		Present	−0.0580	−0.0480	−0.0257	0.0000	0.0035	0.0065
0.101	−0.0253	Exptl.	−0.0477	−0.0443	−0.0406	−0.0198	−0.0032	−0.0045
		Present	−0.0506	−0.0419	−0.0224	−0.0000	0.0031	0.0057
0.112	−0.0253	Exptl.	−0.0439	−0.0423	−0.0406	−0.0198	−0.0032	−0.0063
		Present	−0.0506	−0.0419	−0.0224	0.0000	0.0031	0.0057
0.122	−0.0234	Exptl.	−0.0420	−0.0386	−0.0387	−0.0216	−0.0032	−0.0063
		Present	−0.0468	−0.0388	−0.0208	0.0000	0.0028	0.0053
0.132	−0.0234	Exptl.	−0.0382	−0.0347	−0.0369	−0.0198	−0.0032	−0.0063
		Present	−0.0468	−0.0388	−0.0208	0.0000	0.0028	0.0053
0.153	−0.0219	Exptl.	−0.0325	−0.0310	−0.0330	−0.0216	−0.0032	−0.0045
		Present	−0.0428	−0.0355	−0.0190	0.0000	0.0026	0.0048
0.173	−0.0196	Exptl.	−0.0269	−0.0273	−0.0312	−0.0216	−0.0032	−0.0063
		Present	−0.0392	−0.0325	−0.0174	0.0000	0.0024	0.0044
0.184	−0.0177	Exptl.	−0.0212	−0.0216	−0.0275	−0.0216	−0.0032	−0.0045
		Present	−0.0354	−0.0293	−0.0157	0.0000	0.0021	0.0039
0.194	0.0502	Exptl.	0.0356	0.0387	0.0347	0.0443	0.0683	0.0729
		Present	0.0157	0.0192	0.0305	0.0748	0.0958	0.1042
0.204	0.0502	Exptl.	0.0356	0.0444	0.0347	0.0482	0.0927	0.0766
		Present	0.0157	0.0192	0.0305	0.0748	0.0958	0.1042
0.215	0.0502	Exptl.	0.0317	0.0369	0.0347	0.0500	0.0739	0.0766
		Present	0.0157	0.0192	0.0305	0.0748	0.0958	0.1042
0.235	0.0502	Exptl.	0.0280	0.0350	0.0347	0.0519	0.0720	0.0766
		Present	0.0157	0.0192	0.0305	0.0748	0.0958	0.1042
0.256	0.0502	Exptl.	0.0260	0.0332	0.0347	0.0537	0.0739	0.0766
		Present	0.0157	0.0192	0.0305	0.0748	0.0958	0.1042
0.276	0.0502	Exptl.	0.0260	0.0332	0.0347	0.0557	0.0739	0.0786
		Present	0.0157	0.0192	0.0305	0.0748	0.0958	0.1042

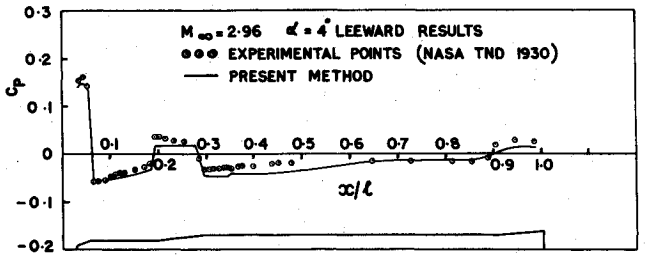

Fig. 2 Pressure distribution for body alone for Mach number 2.96.

for Mach numbers 1 and 2.96 for the entire cone-cylinder-flare-cylinder-flare combination. In computing the results, the experimental values for zero angle of attack are assumed to be 100% accurate.

Table 1 indicates that the agreement is better as one moves away from the leeward side ($\phi = 0°$) toward the windward side ($\phi = 180°$). In addition, some errors may have resulted from the discrepancies in the zero incidence experimental results. For the transonic case, the discrepancy in Fig. 1 over the second flare may be caused by reflected wall disturbances.[3] Satisfactory results also were obtained for a different model for subsonic flow.

In conclusion, it appears that the procedure described here predicts the pressure distribution fairly well for all Mach number ranges and small angles of attack. The results could be improved further, especially for the nose cone part, by improving Eqs. (1) and (2) as suggested in Refs. 1 and 2.

References

[1] Friberg, E.G. and Walchner, O., "Pressure Correlation for Blunted Slender Cones," *AIAA Journal,* Vol. 7, Aug. 1969, pp. 1618-1619.

[2] McBrayer, J.D., "Pressure Distribution about Yawed Cones and Ogives," *Journal of Spacecraft and Rockets,* Vol. 3, June 1966, pp. 940-941.

[3] Kelly, T.C., "Aerodynamic Loading Characteristics at Mach Numbers from 0.80 to 1.20 of a 1/10 Scale Three Stage Scout Model," NASA TND-945, Sept. 1961.

[4] Jernell, L.S., "Aerodynamic Loading Characteristics of a 1/10 Scale Model of the Three Stage Scout Vehicle at Mach Numbers from 1.57 to 4.65," NASA TND-1930, July 1963.

[5] Sastry, M.S., "Application of the Tangent Cone Methods to Transonic Flow Past Axisymmetric Bodies at Small Angles of Attack," *Workshop on Transonic Aerodynamics,* National Aeronautical Lab., Bangalore, India, Dec. 15-17, 1976.